8-4-2021

Quantifying Hydrologic Pathway and Source Connectivity Dynamics in Tile Drainage: Implications for Phosphorus Concentrations

Saeid Nazari
University of Kentucky, saeed_nazari67@yahoo.com

William I. Ford
University of Kentucky, bill.ford@uky.edu

Kevin W. King
U.S. Department of Agriculture

Quantifying Hydrologic Pathway and Source Connectivity Dynamics in Tile Drainage: Implications for Phosphorus Concentrations

Digital Object Identifier (DOI)
https://doi.org/10.1002/vzj2.20154

Notes/Citation Information
Published in *Vadose Zone Journal*, v. 20, issue 5, e20154.

Received: 20 March 2021 | Accepted: 22 June 2021

DOI: 10.1002/vzj2.20154

Vadose Zone Journal

ORIGINAL RESEARCH ARTICLES

Quantifying hydrologic pathway and source connectivity dynamics in tile drainage: Implications for phosphorus concentrations

Saeid Nazari[1] | **William I. Ford**[1] | **Kevin W. King**[2]

[1] Biosystems and Agricultural Engineering, University of Kentucky, Lexington, KY 40509, USA

[2] USDA-ARS, Soil Drainage Research Drainage Unit, Columbus, OH 43201, USA

Correspondence
William Ford, Biosystems and Agricultural Engineering, Univ. of Kentucky, Lexington, KY 40509, USA.
Email: bill.ford@uky.edu

Assigned to Associate Editor Gary Feng.

Abstract

Flowpathways and source water connectivity dynamics are widely recognized to affect tile-drainage water quality. In this study, we developed and evaluated a framework that couples event-based hydrograph recession and specific conductance end-member mixing analysis (SC-EMMA) to provide a more robust framework for quantifying both flow pathway dynamics and source connectivity of drainage water in tile-drained landscapes. High-frequency (30-min) flow and conductivity data were collected from an edge-of-field tile main located in northwestern Ohio, and the newly developed framework was applied for data collected in water year 2019. Multiple linear regression (MLR) analysis was used to evaluate the impact of pathway-connectivity dynamics on flow-weighted mean dissolved reactive P (DRP) concentrations, which were collected as part of the USDA-ARS edge-of-field monitoring network. The hydrograph recession and SC-EMMA results highlighted intra- and interevent differences between quick (preferential) flow and new (precipitation) water transported during events, challenging a common assumption that new water reflects drainage through preferential flow paths. The analysis of hydrologic flow pathways demonstrated matrix–macropore exchange ($Q_{\text{quick-old}}$), preferential flow of new water ($Q_{\text{quick-new}}$), slow flow of old water ($Q_{\text{slow-old}}$), and slow flow of new water ($Q_{\text{slow-new}}$) contributed 9, 39, 42, and 10% to tile discharge, on average, with interevent variability. Matrix water that is transported to tile drains via macropore flowpaths was found to be activated throughout the year, even under drier antecedent conditions, suggesting that matrix–macropore exchange was more sensitive to within-event hydrological processes as compared with antecedent conditions. The MLR results highlighted that pathway-connectivity hydrograph fractions improved prediction of DRP concentrations, although improvement may be more pronounced in landscapes with higher rates of matrix–macropore exchange.

Abbreviations: APEX, Agricultural Policy/Environmental Extender; DRP, dissolved reactive phosphorus; EMMA, end-member mixing analysis; MLR, multiple linear regression; NSE, Nash–Sutcliffe efficiency; SC, specific conductance; SE, storm event

1 | INTRODUCTION

Agricultural subsurface tile drainage across the midwestern United States has increased eutrophication and the persistence of harmful and nuisance algal blooms (Kleinman et al., 2015; Simard et al., 2000; Van Esbroeck et al., 2016). Tile drainage networks in fine-textured soils are often the primary field-scale discharge pathway during stormflows and can disproportionately affect watershed-scale water and nutrient budgets (King et al., 2014; Schilling et al., 2020; Williams et al., 2015). Tile-drainage nutrient loadings during stormflows reflect variability in flow pathway dynamics and source water connectivity (Jiang et al., 2021; King et al., 2015; Ortega-Pieck et al., 2020; Pluer et al., 2020; Smith & Capel, 2018). For the purposes of this study, flow pathway refers to the subsurface flow domain such as percolation through micropores in the soil matrix or preferential transport through macropores, and source connectivity refers to sources of water such as event water (e.g., precipitation or irrigation water), or pre-event water (e.g., water residing in the soil matrix prior to stormflows). Existing methodologies to quantify flow pathway dynamics and source connectivity during storm events have limitations ranging from short temporal domains and coarse sampling resolutions, when using chemical and isotopic tracers (Nazari et al., 2020; Pluer et al., 2020), to uncertainties and long-term data requirements associated with field-scale numerical models (Ford et al., 2017). Development and evaluation of a framework that considers both flow pathway and source connectivity dynamics at the field point of discharge (referred to herein as "edge-of-field") to assess the implications for tile-drain water quality is a major need and research gap.

Soils in tile-drained fields have been conceptualized as two-domain hydrologic systems including diffuse percolation through the soil matrix and preferential flows through macropore networks, with interactions occurring between the domains (Bishop et al., 2015; Brauer et al., 2014; Frey et al., 2016; Gerke et al., 2013; Klaus et al., 2013). Diffuse flow through matrix percolation is associated with slow and delayed seepage of water from the soil matrix to tile drains. Preferential flow through macropores reflects the rapid transfer of water to tiles via desiccation cracks, root channels, worm holes, fractures, and other biopores that bypass percolation through the soil matrix (Beven & Germann, 2013; Flury et al., 1994). There is widespread recognition of bidirectional matrix–macropore interaction during events in tile-drained fields that has been found to significantly affect contaminant loadings (Bishop et al., 2015; Callaghan et al., 2017; Ford et al., 2018; Klaus et al., 2013; Williams et al., 2015). Recent advancements in field-scale hydrology and water quality models (e.g., Hydrus, MACRO, APEX [Agricultural Policy/Environmental Extender], and DRAINMOD) have been important for representing these dynamics and water sources for agroecosystem management (Askar et al., 2020; Beven & Germann, 2013; Ford et al., 2017). However, in agroecosystem models, they often require long-term records for rigorous calibration and validation and neglect or oversimplify simulation of processes including matrix–macropore interaction, resulting in uncertainties during model evaluation (Djabelkhir et al., 2017; Pferdmenges et al., 2020).

Core Ideas

- Hydrograph separation methods are coupled to study tile flow pathway and source connectivity dynamics.
- Results highlight preferential flow of old and new water, bypass recharge, and diffuse flow to tile drainage.
- Sources and pathways of subsurface flow improve prediction of nutrient concentrations.

Utilization of hydrograph recession analysis has been identified as an effective method to quantify event-scale matrix and macropore pathway contributions (Ford et al., 2019; Husic et al., 2019; Nazari et al., 2020). In hydrograph recession, hydrographs are conceptualized as the drainage of a series of reservoirs that have variable hydraulic conductivities and storage volumes (Husic et al., 2019). These reservoirs often recede exponentially, resulting in distinct log-linear regions of the hydrograph. The hydrograph recession method has been successfully applied in subsurface drained landscapes with lateral preferential pathways including karst and tile-drained landscapes to partition flow into diffuse and preferential flowpaths with varying hydraulic conductivities (Ford et al., 2019; Husic et al., 2019; Mellander et al., 2013; Nazari et al., 2020; Schilling & Helmers, 2008).

Regarding tile drainage source dynamics during storm flows, studies have applied various chemical and isotopic tracer methods (Ford et al., 2018; Keinzler & Naef, 2008; Klaus et al., 2013; Vidon & Cuadra, 2010; Williams et al., 2015). Most studies that assess source water dynamics partition tile drainage water into "new" and "old" water components, in which "old" water reflects storage in the soil prior to the event, and "new" water reflects either precipitation or irrigation inputs during an event (Klaus et al., 2013; Schilling & Helmers, 2008; Vidon & Cuadra, 2010; Williams et al., 2016). These studies have found that preferential flow can consist of both new and old water sources (Smith & Capel, 2018; Vidon & Cuadra, 2010; Williams et al., 2016). Although these techniques have been effective at identifying source water dynamics at the field to watershed scale within events, these approaches are often limited to coarse resolution sampling of a few events due to data collection and analytical expense (Pluer et al., 2020; Williams et al., 2016).

Studies have used high-frequency conductance-based measurements as an inexpensive means to continuously monitor source connectivity dynamics during tile-drain hydrologic events at the watershed scale (Heppell & Chapman, 2006; Kronholm & Capel, 2015; Schilling & Helmers, 2008; Vidon & Cuadra, 2010), and more recently at the field scale (Pluer et al., 2020; Smith & Capel, 2018). Specific conductance (SC) can be used as a general indication of runoff age due to change of drainage water ion concentrations during residence within the soil profile. Typically, waters with extended residence times are likely to have a greater ionic content and SC values (Pilgrim & Huff, 1983). In recent years, advances in the robustness and reliability of inexpensive in situ water quality sensors have enabled scientists and practitioners to continuously monitor SC (Snyder et al., 2018). As a result, studies are now deploying these technologies in tile drains at the edge of field and coupling these measurements with end-member mixing analyses (EMMA) to quantify the contribution of preferential flows of new water (Pluer et al., 2020; Smith & Capel, 2018). To date, studies have not coupled hydrograph recession and SC-EMMA approaches for investigating flow pathway and source connectivity dynamics.

Several studies have postulated that flow pathway and source connectivity dynamics impact dissolved reactive P (DRP) loadings in tile-drained agroecosystems. Water-extractable P from soils correlates well with tile drain DRP concentrations during storm events; hence, event water that is rapidly transported to tile via preferential flowpaths is often cited as a driver of tile DRP concentrations (Heathwaite & Dils, 2000; Stamm et al., 1998). Other studies have illustrated that matrix water may be rapidly transported from variable depths in the soil column to tile during events, which alters DRP concentration dynamics (Ford et al., 2018; Klaus et al., 2013; Williams et al., 2016). We postulate that combining hydrograph recession analysis of tile flow and SC-EMMA will improve quantification of flow pathway and source water connectivity dynamics and consequently improve correlations with nutrient concentrations in tile drainage.

The overall objective of this study was to develop a new approach to partition subsurface flow based on both flow pathway and source connectivity descriptors and elucidate their impact on P concentration dynamics in tile drainage. Specific objectives of this manuscript are (a) to apply hydrograph recession analysis of subsurface discharge to partition the tile hydrograph into quick-flow and slow-flow pathways, and SC-EMMA to partition new water and old water; (b) to develop and apply a new hydrograph separation framework that describes both hydrologic pathway (i.e., matrix flow vs. preferential macropore flow) and source connectivity (e.g., new water vs. old water) in tile drainage; and (c) to investigate the relationship between separated hydrograph fractions and tile-drain DRP concentrations.

2 | MATERIALS AND METHODS

2.1 | Study site

A field site from the USDA-ARS Soil Drainage Research Unit edge-of-field monitoring network (Williams et al., 2016) was secured for this study. The field site (0.158 km^2) is a systematically tile drained field in Wood County, Ohio, USA. Systematic tile drainage was implemented at 0.9 m (3 ft) below the soil surface with a lateral spacing of 15.2 m (50 ft). Laterals were routed to a 0.3-m (12-inch) tile main that was equipped with a drainage water management structure before discharging to a downstream ditch (Figure 1a). During our monitoring period, the structure remained open as part of a before–after–control–impact assessment, and thus the field was freely drained. The soils were characterized as silty clay loams consisting of Nappanee (NpA; fine, illitic, mesic Aeric Epiaqualfs) and Hoytville (HcA; fine, illitic, mesic Mollic Epiaqualfs) soil series (Soil Survey Staff, 2019). Soil P levels were measured using Mehlich-3 P soil tests at various depths and locations for the field and were found to average 80.6 mg kg^{-1} in the upper surface layer (0–5 cm), 36.5 mg kg^{-1} from 5 to 15 cm, and 6.3 mg kg^{-1} at depths of 15–60 cm. The typical crop rotation was corn (*Zea mays* L.)–soybean [*Glycine max* (L.) Merr.]–wheat (*Triticum aestivum* L.), managed with conservation tillage. At the onset of monitoring (1 Oct. 2018), the field contained soybean that was harvested on 17 Oct. 2018. The field remained fallow until wheat was planted the following season (11 Oct. 2019).

2.2 | Data collection and analysis

Precipitation and discharge were collected by the USDA-ARS using well-accepted edge-of-field monitoring practices (Williams et al., 2016; Figure 1b). Tipping bucket rain gages were used to measure 10-min rainfall intensity, depth, and duration. Tile mains were equipped with a weir insert (Thel-Mar, Brevard), and an ISCO 4230 bubbler flow meter (Teledyne Isco). Additionally, the tile outlet was equipped with an ISCO 2150 area velocity sensor for 30-min discharge measurements under submerged conditions. Similarly, a surface monitoring site was equipped with a 61-cm (2-ft) H flume and a bubbler flow meter to measure 10-min discharge. Discharge was reported from the standard flume or weir stage–discharge relationships or as the product of area and velocity for the tile outlet when submerged. During water year 2019 (1 Oct. 2018–30 Sept. 2019), total tile discharge was 522 mm, or 41% of precipitation (1,263 mm). Surface runoff was only 8.3 mm (<1% of precipitation), highlighting the importance of the subsurface flow pathway. Mean 30-min tile discharge

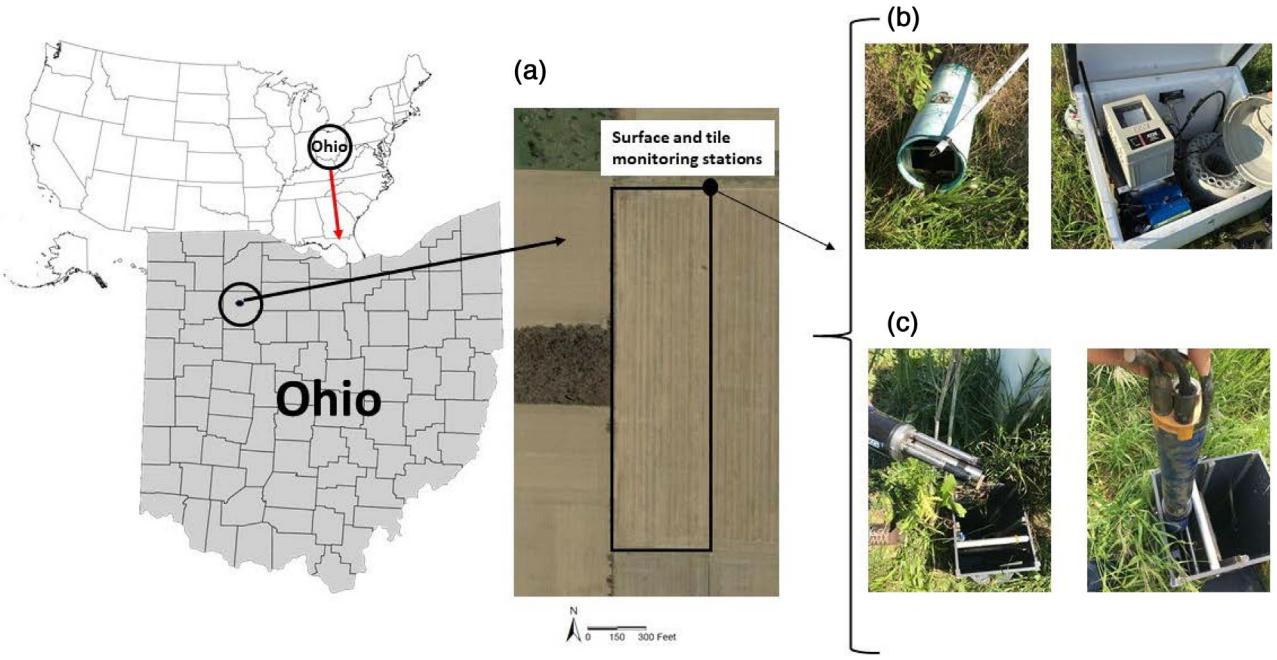

FIGURE 1 Location of the tile-drained field located in Wood County, Ohio, USA. (a) Aerial field delineation and monitoring location. (b) Outlet of the tile network and its installed weir, and ISCO pump sampler. (c) High-frequency sensing YSI EXO2 Sonde and its deployment in a drainage water management structure

throughout the monitoring period was 0.0025 $m^3\ s^{-1}$, whereas maximum discharge was 0.0343 $m^3\ s^{-1}$.

A YSI EXO2 water quality sonde (Xylem/YSI Incorporation, 2020) was installed in the drainage water management structure to continuously (15-min interval) measure specific conductance (see Figure 1c). The sonde was equipped with a conductivity and temperature sensor, which uses four internal pure-nickel electrodes to measure solution conductance. Two of the electrodes are current driven, whereas the other two are used to measure voltage drop (EXO user manual). Monthly maintenance was performed on the instrument per manufacturer recommendations and was consistent with other studies (Snyder et al., 2018). A one-point calibration approach was performed using KorEXO software and a calibration standard with conductivity equal to 1,000 µS cm^{-1}.

Surface and tile water samples were collected using a Teledyne ISCO 6712 portable sampler and accessories. Surface samples were collected using a flow proportional methodology; that is, a 200-ml aliquot was collected for every 1-mm volumetric depth. Ten composited aliquots made up one sample. Due to periodic submergence, a time-proportional approach was used to collect water samples. A 100-ml aliquot was collected every 6 h for 48 h and composited into a single sample bottle reflecting a 2-d composite sample. During rainfall events, samples were collected at higher frequencies (samples collected every 15 min and composited hourly). Collected water samples were analyzed for DRP throughout the monitoring period by first vacuum filtration (0.45 µm) and then analyzing for P using the ascorbic acid reduction method (Murphy & Riley, 1962). Samples rarely fell below method detection limits. Specific conductance was also measured on all Isco collected samples using a calibrated SC sensor in the laboratory.

2.3 | Analytical methodology

2.3.1 | Hydrograph recession and SC-EMMA analysis

Hydrograph recessions from events throughout the monitoring period were compiled to develop a master recession curve. We assumed two flow pathways reflecting reservoirs for matrix and macropore flow, consistent with previous studies (Nazari et al., 2020; Schilling & Helmers, 2008; Vidon & Cuadra, 2010; Williams et al., 2016). Recession coefficients (k) for a linear reservoir are defined by the equation $Q = Q_0 e^{-kt}$ (Gregor & Malik, 2012). The master recession curve (MRC) was automatically created using a genetic algorithm (GA) incorporated in RC 4.0 software (HydroOffice; Gregor & Malik, 2012; Malik & Vojtkova, 2012). We omitted events that were either composed of days with zero flow (i.e., associated with no flux or tile backwater) or had nonlinear recessions associated with disruption of the initial recession and/or secondary flow peaks. For MRC creation, we selected 18 recessions from the site. Then, we selected two linear

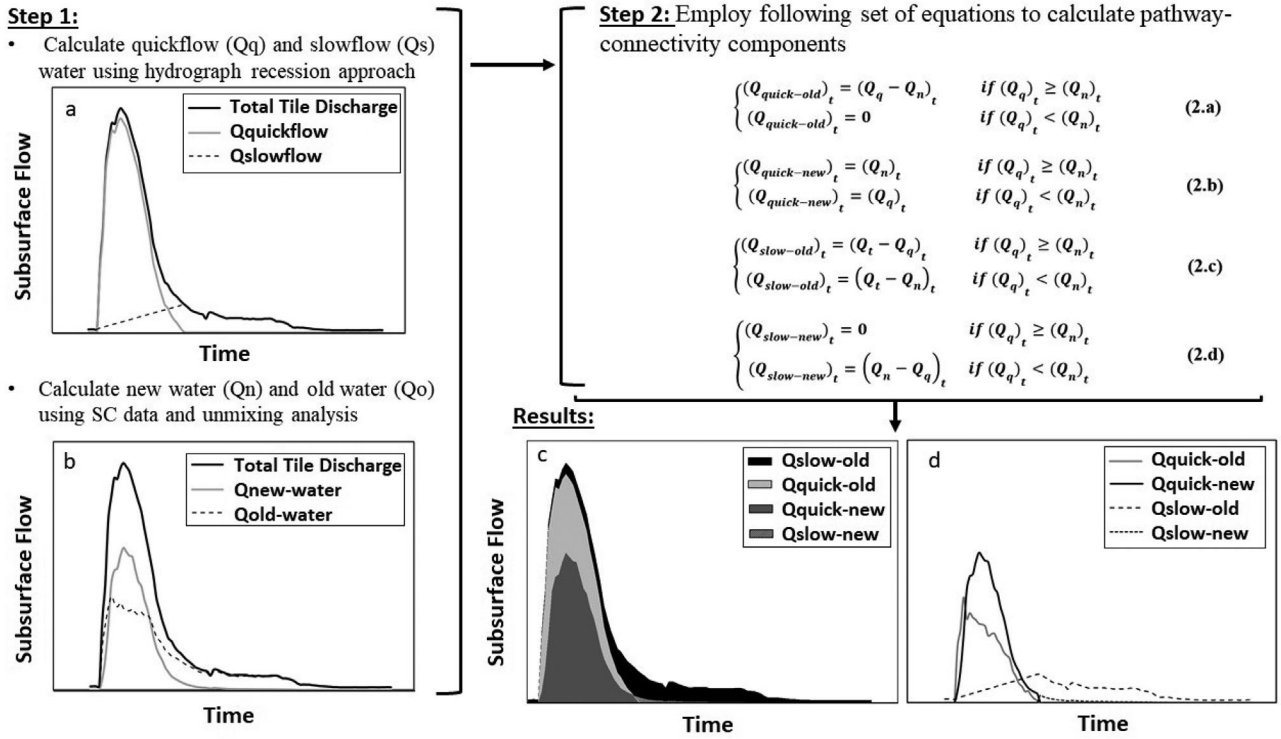

FIGURE 2 Separation of subsurface hydrograph to combined pathway-connectivity components including matrix–macropore exchange ($Q_{\text{quick-old}}$), preferential flow of new water ($Q_{\text{quick-new}}$), old water through slow-flow reservoir ($Q_{\text{slow-old}}$), and new water through slow-flow reservoir ($Q_{\text{slow-new}}$). Subsurface hydrograph is separated into quick flow (Q_{q}) and slow flow (Q_{s}) reservoirs using hydrograph recession analysis in Step 1 (Panel a). Subsurface hydrograph is separated into new water (Q_{n}) and old water (Q_{o}) components using a specific conductance end-member mixing analysis (SC-EMMA) approach (Panel b). In Step 2, a set of equations are employed and calculated Q_{quick}, Q_{slow}, Q_{old} and Q_{new} (from Step 1) are used to separate hydrograph into pathway-connectivity components as shown in Panels c and d

reservoirs and fit two recession curves so that the two recessions provided optimal fit to the data. The goodness-of-fit was tested using Nash–Sutcliffe efficiency (NSE) value (Moriasi et al., 2007).

Hydrograph recession analysis was performed for each storm event using methods described by Husic et al. (2019) and Ford et al. (2019) (Figure 2a), which has been recently applied in tile-drained landscapes (Nazari et al., 2020). Briefly, for each hydrologic event, we graphed the falling limb of the subsurface discharge hydrograph on a logarithmic scale and manually fit linear curves to distinct log-linear regions (reflecting drainage of two reservoirs) to determine the inflection points of the linear trends. Then, a linear increase in slow flow was assumed from the beginning of the rising limb of the hydrograph, which represents the start of quick flow (Q_{quick}), to the determined inflection point on the falling limb from the previous step, which represents the maximum of the slow flow reservoir (Husic et al., 2019). To test the impact of the assumption of linear increase of slow-flow reservoir on flow pathway results, we evaluated two alternative approaches for calculation of the slow-flow hydrograph for eight events. We used a nonlinear two-parameter digital filter method (Eckhardt, 2005), in which parameters were calibrated so that slow-flow reservoir nonlinearly increased to the maximum slow-flow value near or before the hydrograph peak, and then its value remained constant to the inflection point on the falling limb. We also used a nonlinear one-parameter digital filter method (Lyne & Hollick, 1979) in which the recession constant was calibrated so that slow-flow nonlinearly increased slowly early in the event and then increased rapidly towards the inflection point on the falling limb of the hydrograph. Comparing the results of these two approaches showed limited impact on results (1–4% difference from the linear assumption), and the timing of flow pathway peaks remained unchanged. Given the insensitivity of this assumption, we present results using the simplified linear assumption for the 27 events. The area between the hydrograph and the slow flow curve represented Q_{quick}, and the area underneath the slow flow reservoir curve represented Q_{slow}. We performed this analysis on 27 storm events (SEs) from water year 2019.

New water and old water fractions were quantified using specific conductance end-member mixing analysis (SC-EMMA; Figure 2b). Following the approach of Smith and Capel (2018), we solved the following system of equations at each time step in order to estimate the pre-event and event

flow contributions to tile drainage.

$$\left(Q_{\text{Tile}}\right)_t = \left(Q_{\text{old}}\right)_t + \left(Q_{\text{new}}\right)_t \tag{1a}$$

$$\left(\text{SC}_{\text{Tile}}\right)_t\left(Q_{\text{Tile}}\right)_t = \text{SC}_{\text{old}}\left(Q_{\text{old}}\right)_t + \text{SC}_{\text{new}}\left(Q_{\text{new}}\right)_t \tag{1b}$$

where, $(Q_{\text{Tile}})_t$, $(Q_{\text{old}})_t$, $(Q_{\text{new}})_t$ were total, old water, and new water tile discharges at time t, respectively. $(\text{SC}_{\text{Tile}})_t$ was the measured specific conductance of subsurface tile water at time t, and $(\text{SC}_{\text{old}})_t$ and $(\text{SC}_{\text{new}})_t$ were specific conductance of old water and new water at time t, respectively. We assumed that SC_{new} was the average specific conductance of surface water runoff samples collected from the surface site, and SC_{old} was the specific conductance of subsurface water at the beginning of each event and varied from one event to the next, a result of variable soil water conditions.

2.3.2 | Hydrograph separation framework

We developed a new hydrograph separation framework that considers both flow pathway and water source connectivity (Figure 2c, d). Once Q_{quick}, Q_{slow}, Q_{new}, and Q_{old} were calculated, we developed the following piecewise functions for each time step (t) to estimate the portion of old water that drains to the quick-flow reservoir ($Q_{\text{quick-old}}$), the portion of new water that drains to the quick-flow reservoir ($Q_{\text{quick-new}}$), the portion of new water that drains through the slow-flow reservoir ($Q_{\text{slow-new}}$), and the portion of old water that drains to the slow-flow reservoir ($Q_{\text{slow-old}}$). In deriving this framework, we assumed that (a) if quick flow exceeded new water, all new water was attributed to the quick-flow pathway, and (b) if new water exceeded quick flow, then all quick flow was attributed to new water. Based on these assumptions, each pathway-source component of the hydrograph can be calculated as follows:

$$\begin{cases} \left(Q_{\text{quick-old}}\right)_t = \left(Q_{\text{quick}} - Q_{\text{new}}\right)_t & \text{if } \left(Q_{\text{quick}}\right)_t \geq \left(Q_{\text{new}}\right)_t \\ \left(Q_{\text{quick-old}}\right)_t = 0 & \text{if } \left(Q_{\text{quick}}\right)_t < \left(Q_{\text{new}}\right)_t \end{cases} \tag{2a}$$

$$\begin{cases} \left(Q_{\text{quick-new}}\right)_t = \left(Q_{\text{new}}\right)_t & \text{if } \left(Q_{\text{quick}}\right)_t \geq \left(Q_{\text{new}}\right)_t \\ \left(Q_{\text{quick-new}}\right)_t = \left(Q_{\text{quick}}\right)_t & \text{if } \left(Q_{\text{quick}}\right)_t < \left(Q_{\text{new}}\right)_t \end{cases} \tag{2b}$$

$$\begin{cases} \left(Q_{\text{slow-old}}\right)_t = \left(Q_{\text{total}} - Q_{\text{quick}}\right)_t & \text{if } \left(Q_{\text{quick}}\right)_t \geq \left(Q_{\text{new}}\right)_t \\ \left(Q_{\text{slow-old}}\right)_t = \left(Q_{\text{total}} - Q_{\text{new}}\right)_t & \text{if } \left(Q_{\text{quick}}\right)_t < \left(Q_{\text{new}}\right)_t \end{cases} \tag{2c}$$

$$\begin{cases} \left(Q_{\text{slow-new}}\right)_t = 0 & \text{if } \left(Q_{\text{quick}}\right)_t \geq \left(Q_{\text{new}}\right)_t \\ \left(Q_{\text{slow-new}}\right)_t = \left(Q_{\text{new}} - Q_{\text{quick}}\right)_t & \text{if } \left(Q_{\text{quick}}\right)_t < \left(Q_{\text{new}}\right)_t \end{cases} \tag{2d}$$

We partitioned the tile flow into $Q_{\text{quick-new}}$, $Q_{\text{quick-old}}$, $Q_{\text{slow-new}}$, and $Q_{\text{slow-old}}$ for the entire 2019 water year. For each selected event (27 events), we calculated total water volume and fractions for each partitioning.

2.3.3 | Comparison with nutrient concentrations

Dissolved reactive P concentrations (DRP_{tile}) in tile drainage will reflect mixing of flow contributions and their associated nutrient compositions, which can be described using a linear mass-balance mixing model. Based on our pathway-connectivity framework, we conceptualized tile drain nutrient concentrations to be influenced by the four hydrograph fractions as follows:

$$\begin{aligned} \text{DRP}_{\text{tile}}Q_{\text{tile}} = {} & \text{DRP}_{\text{quicknew}}Q_{\text{quicknew}} + \text{DRP}_{\text{quickold}}Q_{\text{quickold}} \\ & + \text{DRP}_{\text{slownew}}Q_{\text{slownew}} + \text{DRP}_{\text{slowold}}Q_{\text{slowold}} \end{aligned} \tag{3}$$

where DRP is the daily flow-weighted mean nutrient concentration (mg L^{-1}), and Q is the tile flowrate for each partition (mm d^{-1}). We used a daily, as opposed to event-based time step since cumulative event dynamics will smooth out some variability in pathway dynamics. We also disregarded the sorption–desorption effects along the pathways for simplification and because the time scale of the events was short. Hence, our analysis reflects average DRP concentrations for each pathway across events.

Dividing both sides of the Equation 3 by Q_{Tile}, the equation can be written as a multiple linear regression (MLR) model, with DRP_{tile} as the measured dependent variable, fractions of pathway-source contributions as independent variables, and concentrations of the sources as unknowns:

$$\begin{aligned} \text{DRP}_{\text{tile}} = {} & F_{\text{quicknew}}\text{DRP}_{\text{quicknew}} + F_{\text{quickold}}\text{DRP}_{\text{quickold}} \\ & + F_{\text{slownew}}\text{DRP}_{\text{slownew}} + F_{\text{slowold}}\text{DRP}_{\text{slowold}} \end{aligned} \tag{4}$$

where F is the fraction of total tile discharge for each partition at a given time step.

Daily subsurface DRP loadings and flow from the tile drainage network were calculated for all events throughout the monitoring period. We determined the midpoint of all sample time steps for each collected water sample, then used linear interpolation between measured values at the midpoint to estimate the concentration for each interval, and finally estimated loading as the product of interpolated concentrations

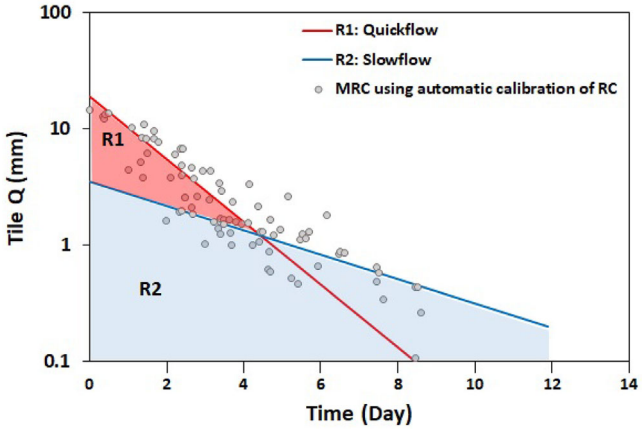

FIGURE 3 Master recession curve constructed from 18 subsurface flow recessions for water year 2019. R1 and R2, Reservoirs 1 and 2; MRC, master recession curve; RC, recession curve; *Q*, tile discharge

and flow rate (Williams et al., 2015). We calculated daily *Q*quick-new, *Q*quick-old, *Q*slow-new, and *Q*slow-old by summing calculated 30-min flow components. Daily flow-weighted mean concentrations of DRP were calculated by dividing daily nutrient load by daily tile discharge. Daily flow-weighted mean concentration of DRP was used for MLR analysis in Equation 4.

We performed a MLR at a daily time step in order to estimate "best-fit" concentrations for the partitioned hydrograph sources. The MLR models were performed in RStudio software. The *F* statistic was used to test the null hypothesis that individual coefficients (DRP values in Equation 4) were not equal to zero, as well as the null hypothesis that the overall MLR model provided a superior fit to a mean trend. The *p* values were calculated for the *F* statistics in both hypothesis testing scenarios, and significance results are reported for $p < .05$, $p < .01$, $p < .001$, and $p < .0001$. We performed an analogous analysis using only Q_{quick}/Q_{slow} and Q_{new}/Q_{old} to assess the improvement in predictions when using our new coupled hydrograph separation framework over each isolated hydrograph separation method.

3 | RESULTS AND DISCUSSION

3.1 | Hydrograph recession and SC-EMMA results

Master recession curve analysis for the 2019 water year data resulted in two discernable reservoirs reflecting preferential flow through macropores and diffuse drainage through the soil matrix (Figure 3). Reservoir 1 (R1) reflected a steeply recessing quick-flow pathway, whereas Reservoir 2 (R2) was characteristic of a mildly recessing slow-flow pathway. The recession coefficients for R1 and R2 were 0.9 and 0.25 d^{-1}, respectively (Figure 3). The NSE value was equal to 0.81, suggesting very good fit (Moriasi et al., 2007). Given that the recession coefficients vary by greater than threefold (Husic et al., 2019; Rimmer & Hartmann, 2012; Schilling & Helmers, 2008), these finding are indicative of two distinct flow pathways. Results of the master recession curve suggest that R1 accounted for 54% of the subsurface flow while the remainder, or 46% was attributed to R2. These values were consistent with ranges reported for preferential and diffuse flow at nearby loam and clay fields with similar long-term management practices (Ford et al., 2017; Nazari et al., 2020) and indicated that both preferential and matrix flow are significant contributors to subsurface drainage.

Specific conductance (SC) measurements during storm events showed a consistent pattern of maximum values occurring prior to the event, a decrease to minimum values slightly before or after peak discharge, and then increasing values on the receding limb toward pre-event levels (Figure 4). Pre-event SC averaged 566.5 μS cm^{-1} for the 27 events. Minimum event SC averaged 240.5 μS cm^{-1}, reflecting decreases towards values reported for precipitation (e.g., 12 μS cm^{-1} in Smith & Capel, 2018) and measured SC in the surface runoff samples (15 μS cm^{-1} from 55 surface runoff samples). Interestingly, the time to minimum SC values differed significantly for fall and winter events (mean = 698 min; with range of 165–1,260 min) compared with spring and summer events (mean = 183 min, with a range of 60–390 min). Similar quick responses (141 min) from spring and summer events on silty clay loam sites in Iowa (Smith & Capel, 2018) have been reported and may be associated with differences in management practices, precipitation patterns, and seasonal differences in preferential flow paths (Graham & Lin, 2011; Pluer et al., 2020; Williams et al., 2016).

Based on our results, we postulate seasonal differences and precipitation pattern dynamics both play an important role in timing of new water delivery to tile drains. Regarding precipitation patterns, our results showed that average event precipitation intensity (PI) in summer and spring (PI = 9.8 mm d^{-1}) were twofold greater than for the events in fall and winter (PI = 4.2 mm d^{-1}). With regard to seasonal environmental conditions, previous studies in tile-drained landscapes suggest that during the growing season, low-moisture conditions promote desiccation crack expansion, which enables water to rapidly transfer to tiles or bypass the drainage system (Nazari et al., 2020). Conversely, during winter, a large amount of infiltration can occur via preferential flow because under partially saturated conditions a considerable portion of macropores remain air filled (Granger et al., 1984; Mohammed et al., 2018; Pittman et al., 2020; Stadler et al., 2000). Nevertheless, infiltrated meltwater may freeze due to matrix–macropore heat and water transfer, and the frozen water can block the macropore pathway, and consequently reduce infiltration of

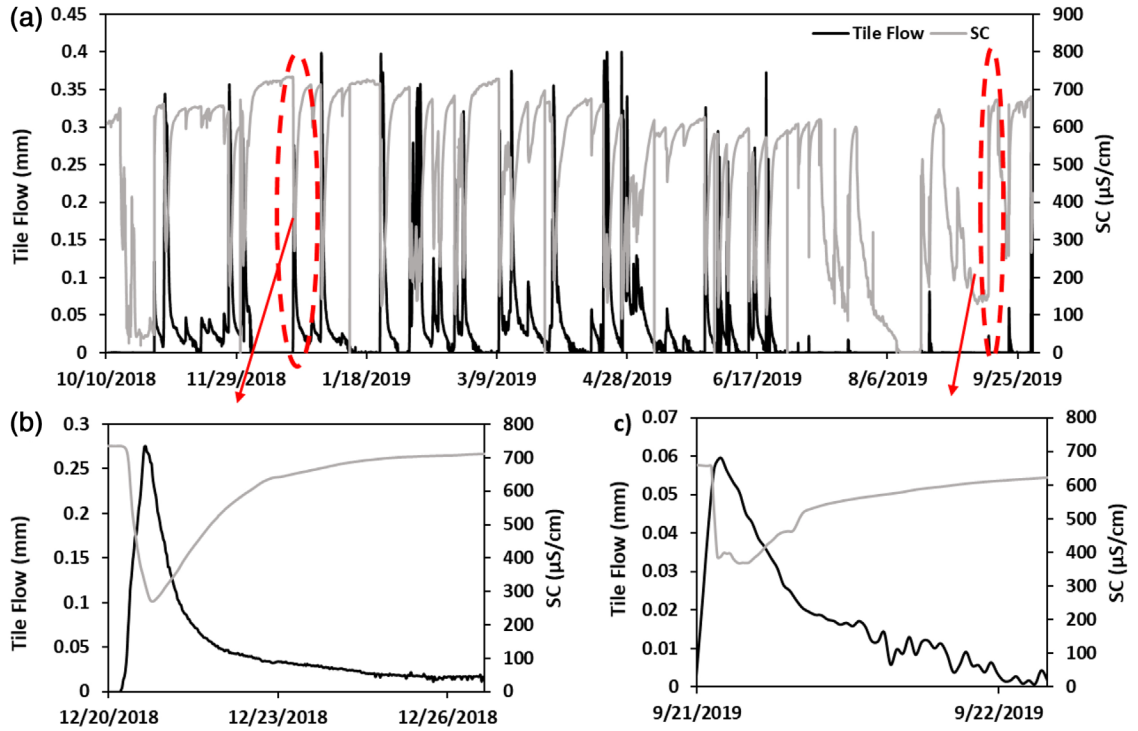

FIGURE 4 (a) Time series of data including 30-min tile flow (mm) and 15-min specific conductance (SC, µS cm^{-1}). Two events are highlighted at different times of year including (b) fall and (c) summer

event water (Demand et al., 2019; Mohammed et al., 2021; Stadler et al., 1997; Watanabe & Kugisaki, 2017). Cumulatively, these seasonal environmental factors in precipitation and soil dynamics are likely drivers of short time to peaks in spring and summer and longer time to peaks in fall and winter.

Results of the event-based continuous recession and SCEMMA analysis illustrated noticeable differences in magnitude and timing of the quick flow and new water fractions, challenging the assumption that new water is equivalent to preferential flow (Table 1, Figure 5). Cumulatively, Q_{quick} was estimated to be 172 mm (48% of total tile discharge) and Q_{new} was estimated to be 176 mm (49% of total tile discharge). For individual events, we found quick-flow contribution to total subsurface flow varied from 8 to 77%, and new water contributions varied from 3 to 82% (Table 1). However, new water and quick-flow hydrographs often differed in terms of peak timing and magnitude between events (Figure 5). The peak of Q_{quick} often occurred before Q_{new} except for SE12 and SE26. The difference between time to peak of Q_{quick} and Q_{new} averaged 164 min for fall and winter events, and 87 min for spring and summer events. Studies have often assumed the amount of preferential flow is equated to the amount of new water transported to tile (Klaus et al., 2013). For example, Smith and Capel (2018) and Pluer et al. (2020) interpreted conductance-based unmixing results as separation of preferential flow and slow flow. Similarly, Williams et al. (2016) used $\delta^{18}O$ to define event and pre-event water to tile drains and assumed that event water transported to tile drains within a storm event was only possible through macropore flows. Our findings suggest that new water during storm flows may be transported to tile through both preferential and diffuse flow paths, suggesting caution should be used with tracer-based approaches.

3.2 | Pathway-connectivity results

Results of the pathway-connectivity framework indicates all four hydrograph components had a significant, but variable contribution to tile hydrology. Cumulatively, $Q_{quick\text{-}old}$, $Q_{quick\text{-}new}$, $Q_{slow\text{-}old}$, and $Q_{slow\text{-}new}$ contributed 9, 39, 42, and 10% of tile discharge for the analyzed events (Table 1). The $Q_{quick\text{-}old}$ contributions ranged from 0.05 to 27%, $Q_{quick\text{-}new}$ contributions ranged from 1.86 to 66%, $Q_{slow\text{-}new}$ contributions ranged from 0.7 to 33%, and $Q_{slow\text{-}old}$ contributions ranged from 13 to 98% of total tile discharge. Many agroecosystem water management models make simplifying assumptions that limit their ability to represent the abovementioned pathway-connectivity dynamics. For instance, APEX, DRAINMOD-P, ADAPT (Agricultural Drainage and Pesticide Transport), RZWQM2-P (Root Zone Water Quality Model-Phosphorus), SimplyP (a Simple Phosphorus Model), SWAP (Soil Water Atmosphere Plant), and SWAT (Soil and

TABLE 1 Summary of event timings, precipitations, total tile discharges, and flow partitioning results

Event no.	Event start time	Event ending time	Event precip.	Q_{Tile}	Q_{quick}	Q_{slow}	Q_{new}	Q_{old}	$Q_{quick\text{-}old}$	$Q_{quick\text{-}new}$	$Q_{slow\text{-}old}$	$Q_{slow\text{-}new}$
			mm									
SE1	1 Nov. 2018, 0100 h	9 Nov. 2018, 1000 h	49.91	33.2 (870)	21.5 (870)	11.7 (4,020)	13.1 (1,380)	20.1 (690)	8.9 (690)	12.6 (1,380)	11.2 (3,750)	0.5 (4,020)
SE2	9 Nov. 2018, 1330 h	12 Nov. 2018, 0330 h	8.43	4 (300)	0.5 (300)	3.5 (1,230)	0.1 (990)	3.9 (300)	0.4 (300)	0.1 (300)	3.5 (1,140)	0 (1,200)
SE3	26 Nov. 2018, 0100 h	30 Nov. 2018, 0400 h	23.86	21.8 (780)	13.5 (780)	8.2 (2,850)	12.3 (840)	9.5 (510)	2.2 (510)	11.4 (840)	7.4 (2,190)	0.9 (2,850)
SE4	1 Dec. 2018, 1100 h	5 Dec. 2018, 2230 h	14.21	16.9 (930)	7.9 (900)	9 (2,880)	7.7 (960)	9.2 (900)	1.2 (900)	6.7 (960)	8 (2,310)	1 (2,880)
SE5	20 Dec. 2018, 1230 h	27 Dec. 2018, 0400 h	22.4	16.4 (990)	7.8 (960)	8.5 (2,610)	6.2 (1,080)	10.2 (930)	2.7 (720)	5.2 (1,080)	7.5 (2,100)	1 (2,610)
SE6	27 Dec. 2018, 1300 h	31 Dec. 2018, 0700 h	6.44	5.5 (1,440)	0.9 (1,410)	4.6 (2,640)	0.4 (1,560)	5.2 (1,410)	0.7 (1,410)	0.3 (1,560)	4.5 (2,550)	0.1 (2,580)
SE7	31 Dec. 2018, 0730 h	5 Jan. 2019, 2330 h	24.56	21.9 (540)	12.7 (540)	9.2 (2,850)	12.1 (660)	9.8 (450)	1.8 (450)	10.9 (660)	8 (2,010)	1.2 (2,820)
SE8	22 Jan. 2019, 2230 h	31 Jan. 2019, 0700 h	39.55	34.8 (570)	26.8 (2,580)	8 (6,000)	24.2 (2,730)	10.7 (2,310)	3.8 (300)	23.1 (720)	6.9 (3,060)	1.1 (3,960)
SE9	12 Feb. 2019, 1030 h	14 Feb. 2019, 1200 h	14.18	5.7 (1,080)	1.8 (1,080)	3.9 (1,860)	2.3 (1,140)	3.4 (990)	0.3 (990)	1.5 (1,140)	3.2 (1,230)	0.7 (1,860)
SE10	14 Feb. 2019, 2330 h	19 Feb. 2019, 1700 h	1.23	9.7 (990)	3.9 (990)	5.8 (2,160)	4.4 (990)	5.3 (210)	0.2 (180)	3.6 (990)	5.1 (1,140)	0.7 (2,160)
SE11	20 Feb. 2019, 1430 h	21 Feb. 2019, 1004 h	8.44	4.4 (570)	2.7 (540)	1.7 (990)	3.6 (570)	0.8 (300)	0.2 (300)	2.5 (540)	0.6 (420)	1.1 (990)
SE12	23 Feb. 2019, 1630 h	26 Feb. 2019, 0330 h	6	12.6 (1,050)	8.3 (1,400)	4.4 (2,490)	7.2 (1,110)	5.4 (750)	1.5 (750)	6.8 (1,110)	4 (1,980)	0.4 (2,490)
SE13	9 Mar. 2019, 1630 h	13 Mar. 2019, 0800 h	21.38	12.4 (660)	5 (660)	7.4 (1,530)	8 (690)	4.4 (330)	0.3 (330)	4.8 (660)	4.1 (750)	3.2 (1,530)
SE14	14 Mar. 2019, 1530 h	20 Mar. 2019, 0900 h	11.43	25 (1,890)	8.2 (1,890)	16.8 (3,660)	9.7 (1,980)	15.3 (1,830)	1.2 (1,830)	7.1 (1,940)	14.2 (2,730)	2.6 (3,630)
SE15	20 Mar. 2019, 1800 h	26 Mar. 2019, 1730 h	17.4	11 (600)	2.7 (600)	8.3 (2,880)	1.8 (870)	9.2 (480)	1.4 (480)	1.3 (870)	7.8 (2,250)	0.5 (2,880)
SE16	28 Mar. 2019, 0530 h	4 Apr. 2019, 0330 h	37.18	27.2 (2,370)	13.4 (4,080)	13.8 (6,630)	13.8 (4,200)	13.5 (3,450)	2.2 (1,740)	11.2 (2,490)	11.2 (3,360)	2.6 (4,320)

(Continues)

TABLE 1 (Continued)

Event no.	Event start time	Event ending time	Event precip.	Q_{Tile}	Q_{quick}	Q_{slow}	Q_{new}	Q_{old}	$Q_{quick\text{-}old}$	$Q_{quick\text{-}new}$	$Q_{slow\text{-}old}$	$Q_{slow\text{-}new}$
SE17	18 Apr. 2019, 1530 h	20 Apr. 19, 0404 h	33.71	16.1 (900)	6.3 (900)	9.8 (1,590)	11.2 (960)	4.9 (480)	0.4 (480)	6 (900)	4.5 (780)	5.3 (1,590)
SE18	20 Apr. 2019, 0500 h	25 Apr. 2019, 0726 h	13.92	23.2 (210)	8.5 (300)	14.7 (30)	13.7 (330)	9.5 (210)	0 (210)	8.5 (300)	9.5 (180)	5.2 (450)
SE19	27 Apr. 2019, 1830 h	29 Apr. 2019 1530 h	17.02	12.7 (390)	5.2 (630)	7.6 (1,620)	5.3 (690)	7.4 (540)	0.6 (300)	4.5 (450)	6.8 (870)	0.8 (1,380)
SE20	30 Apr. 2019, 1400 h	1 May 2019, 1330 h	6.04	4.4 (240)	0.6 (270)	3.8 (810)	0.7 (360)	3.8 (240)	0.2 (270)	0.4 (360)	3.5 (570)	0.3 (780)
SE21	13 May 2019, 0630 h	16 May 2019, 2200 h	3.7	4.4 (210)	0.5 (210)	4 (1,170)	0.5 (330)	3.9 (180)	0.2 (180)	0.3 (330)	3.7 (810)	0.3 (1,140)
SE22	28 May 2019, 0400 h	31 May 2019, 1228 h	8.27	10.1 (150)	2.5 (150)	7.7 (60)	5.3 (210)	4.9 (150)	0 (150)	2.5 (210)	4.9 (150)	2.8 (60)
SE23	13 June 2019, 1900 h	14 June 2019, 2330 h	2.18	3.9 (120)	1.4 (240)	2.5 (600)	2.1 (270)	1.8 (210)	0.3 (60)	1 (120)	1.4 (90)	1.1 (450)
SE24	15 June 2019, 1030 h	19 June 2019, 1330 h	5.45	11.6 (1,140)	5.6 (1,140)	6 (2,220)	6.1 (1,170)	5.5 (1,140)	0.6 (540)	5 (1,170)	4.9 (1,140)	1.1 (2,220)
SE25	6 July 2019, 1930 h	10 July 2019, 0930 h	16.77	0.6 (90)	0.1 (90)	0.6 (210)	0 (150)	0.6 (90)	0 (90)	0 (150)	0.6 (270)	0 (210)
SE26	21 Sept. 2019, 1500 h	22 Sept. 2019, 1900 h	22.91	1 (120)	0.5 (120)	0.5 (600)	0.3 (60)	0.7 (90)	0.25 (90)	0.25 (120)	0.47 (540)	0.03 (600)
SE27	30 Sept. 2019, 0200 h	30 Sept. 2019, 2330 h	32.76	6.2 (300)	3.1 (240)	3.1 (870)	3.5 (570)	2.7 (270)	1.2 (270)	1.9 (480)	1.6 (480)	1.5 (870)
Sum			469.33	356.83	171.87	184.96	175.32	181.5	32.54	139.13	148.98	35.99
Mean			17.38	13.21	6.37	6.86	6.50	6.73	1.21	5.16	5.52	1.33
SD			±12.5	±9.5	±6.5	±4.1	±5.8	±4.67	±1.8	±5.27	±3.47	±1.41

Note. Numbers in parentheses represent time to peak in minutes. SE, storm event. In this table, Q_{Tile}, Q_{quick}, Q_{slow}, Q_{new}, Q_{old}, $Q_{quick\text{-}old}$, $Q_{quick\text{-}new}$, $Q_{slow\text{-}old}$, and $Q_{slow\text{-}new}$ represent total tile flow, quick flow, slow flow, new water, old water, matrix–macropore exchange, preferential flow of new water, old water through slow-flow reservoir, and new water through slow-flow reservoir, respectively.

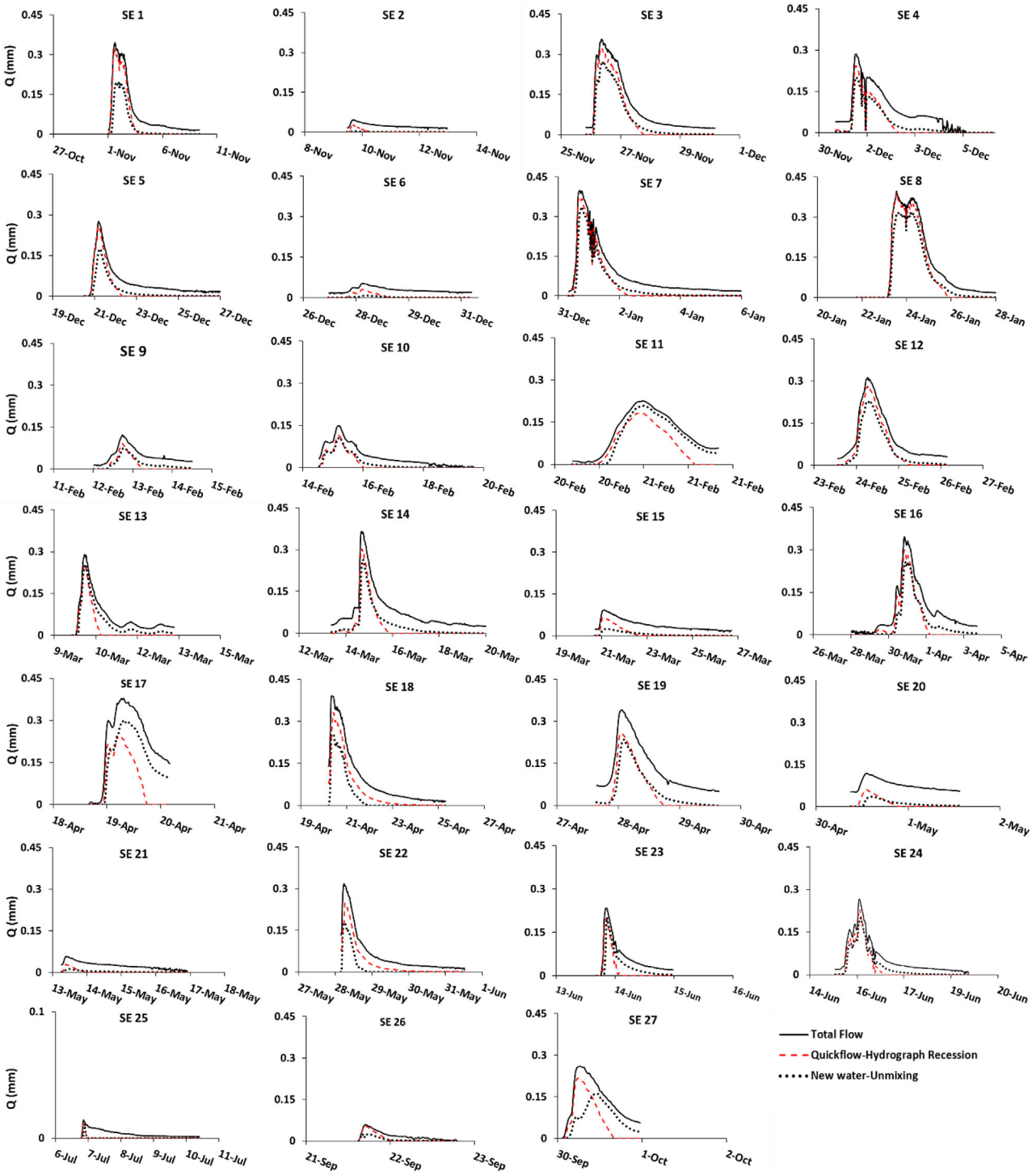

FIGURE 5 Tile discharge (Q), quick flow calculated using hydrograph recession analysis, and new water calculated using specific conductance end-member mixing analysis for each storm event (SE) at the study site during water year 2019

Water Assessment Tool) do not actively simulate matrix–macropore processes explicitly through dual-porosity or dual-permeability frameworks (Pferdmenges et al., 2020). This is important not only for hydrologic simulations, but also contaminant transport given source connectivity has a major impact on nutrient, pesticide, and sediment transport processes, as will be discussed in Section 3.3. As modeling frameworks in agroecosystems evolve to incorporate robust hydrologic processes, the coupled hydrograph-recession SC-EMMA framework proposed herein may be useful for quantitative model evaluations given the heterogeneity observed at the event-scale in pathway-connectivity dynamics.

Results for $Q_{\text{quick-new}}$ support existing perceptions that preferential transport of surface water occurs through both

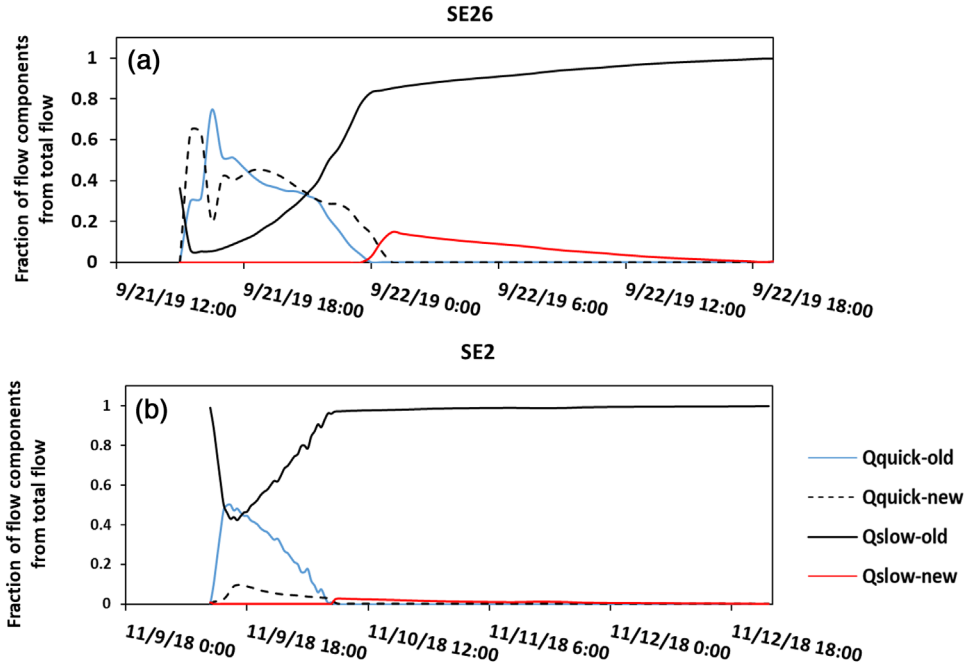

FIGURE 6 Results of pathway connectivity framework for (a) Storm Event 26 (SE26) and (b) SE2. These two events were selected from summer and fall because they reveal seasonal differences in subsurface flow pathway and source connectivity. In this figure, $Q_{\text{quick-old}}$, $Q_{\text{quick-new}}$, $Q_{\text{slow-old}}$, and $Q_{\text{slow-new}}$ represent matrix–macropore exchange, preferential flow of new water, old water through slow-flow reservoir, and new water through slow-flow reservoir, respectively

saturated and unsaturated conditions through macropores in fine-textured, tile-drained soils. The $Q_{\text{quick-new}}$ for the 27 events had a positive linear relationship with event precipitation (R^2 = .4), and a weak negative correlation with 10-d antecedent rainfall (R^2 = .12). Further, under low antecedent conditions in summer (Figure 6a), two *Q*quick-new peaks were observed, one of which occurred 60 min into the event, and the other occurred 210 min into the event. This finding illustrates that fine-textured tile-drained landscapes are not solely drained by binary flow reservoirs but instead reflect a spectrum of slow to rapid flows. For example, Schilling et al. (2008) illustrated recessions in tile-drained landscapes of Iowa may be separated into quick, intermediate, and slow flow regimes. The timing of the second peak is reflective of the time to peak for *Q*quick-new in fall as evidenced by similar magnitude drainage events with greater antecedent moisture (Figure 6b). Although further work is needed to illustrate the prominence and mechanisms driving these early-event peaks, one potential mechanism is that desiccation crack networks may be more prominent during these low antecedent moisture periods, promoting unsaturated film flow to tiles (Ford et al., 2017; Mirus & Nimmo, 2013 Nimmo, 2012). Regardless, these findings support a growing body of research in tile-drained landscapes that suggest macropore flows of surface-derived water sources are significant under a range of antecedent moisture conditions (Cey & Rudolph, 2009; Ford et al, 2017; Smith & Capel, 2018; Tokunga & Wan, 1997).

Results for quick flow of old water ($Q_{\text{quick-old}}$) highlight the importance of intrinsic event properties to control the magnitude of matrix–macropore flow. The $Q_{\text{quick-old}}$ component of the hydrograph, by definition, reflects matrix water that is transported to tile-drains via macropore flowpaths and was found to be activated throughout the year, even under drier antecedent conditions. Like $Q_{\text{quick-new}}$, we found a positive linear relationship between $Q_{\text{quick-old}}$ and precipitation (R^2 = .52), and a weak negative relationship with 10-d antecedent rainfall (R^2 = .08). We also found $Q_{\text{quick-old}}$ to have a positive linear relationship with $Q_{\text{quick-new}}$ (R^2 = .40). Klaus et al. (2013) performed irrigation experiments on a tile-drained hillslope and found old water was mobilized through shallow surface soil depths (20–40 cm) and transported through macropores because macropore–matrix interaction leads to an initiation of macropore flow after a moisture threshold was exceeded. Several other studies have highlighted macropore flow under porewater tension conditions and associated importance of macropore–matrix interaction in controlling this flow (Bishop et al., 2015; Callaghan et al., 2017; Cey & Rudolph, 2009; Tokunaga & Wan, 1997). The findings of our study support that increasing preferential flow of new water enhances mixing with the soil matrix (i.e., bidirectional matrix–macropore interaction). Likewise, our findings support that larger precipitation events will result in greater saturation of soils and thus greater rates of matrix–macropore exchange. Contrary to anticipated outcomes, antecedent rainfall had little impact on

matrix–macropore exchange. This finding suggests that antecedent conditions may be insensitive when compared with intrinsic storm event hydrologic characteristics with regards to magnitude of matrix–macropore exchange.

Apart from near-surface initiation of macropore flow, rapid transport of old water to tile drains could occur because of rapid transition of the capillary fringe from tension saturation to positive pressure (Sklash & Farvolden, 1979). In tile-drained systems, the groundwater elevation is at or near the tile drain elevation; therefore, it is possible that part of the correlation between macropore flow and matrix–macropore exchange is associated with the rapid transition of the capillary fringe tension saturation to positive pressure near tile drains. Nevertheless, as will be discussed in Section 3.3, we do not feel this is a prominent source for our study since regression analyses with DRP concentrations indicated high levels of DRP in the $Q_{\text{quick-old}}$ pathway.

Our findings show contributions of both new water and old water to the slow flow pathways, suggesting that groundwater recharge of new water plays an important role in tile drainage fluxes. The average time to peak of $Q_{\text{slow-new}}$ for all the events was 32 ± 4 h. Using a one-dimensional form of Darcy's law in which we assumed area weighted hydraulic conductivity averaged 5.5 cm d^{-1} and 45% of porosity for our site (Soil Survey Staff, 2019; Vidon & Cuadra, 2010), we found that for new stormwater to reach tile drains through diffuse percolation alone could take on the order of a week. This result suggests that new water, at least to some degree, bypasses portions of the soil matrix before ultimately draining through the soil drainage reservoir. Previous studies have indicated that unsaturated-zone preferential flow can significantly contribute to groundwater recharge (Cuthbert et al., 2013; Lee et al., 2006; Mirus & Nimmo, 2013). For tile-drained landscapes, Frey et al. (2012) highlighted that under partially saturated conditions, water transport via macropores to subsurface can then be laterally transmitted to tiles via short slow-flow pathways in the vicinity of tile lines. Although we did not measure groundwater level and its responsiveness to preferential flow, we found that there was a negative relationship between $Q_{\text{slow-new}}$ time to peak and 10-d antecedent rainfall ($R^2 = .19$). This finding is consistent with Lee et al. (2006), where the authors found that groundwater recharge with preferential flow is dependent on both thickness and degree of saturation of the unsaturated zone. Collectively, these results suggest that groundwater recharge could be an important regulator of timing and flow pathway dynamics in tile discharge.

3.3 | Implications for P delivery at the edge of field

Daily flow-weighted mean DRP concentrations were poorly correlated with discharge, stemming primarily from significant variability at low tile discharges (Figure 7). We found that tile drainage only predicted about 10% of the variability in DRP. The simple regression underestimates DRP concentrations at low-flow conditions where DRP concentration was highly variable and overestimated DRP concentrations at high-flow conditions when concentrations were less variable. This finding suggests that during high-flow conditions, subsurface discharge can be a more reliable predictor of DRP concentration, whereas under low-flow conditions, other environmental factors may influence DRP such as P (de)sorption, redox conditions, and water source (King et al., 2015; Kleinman & Sharpley, 2002; Wright et al., 2001).

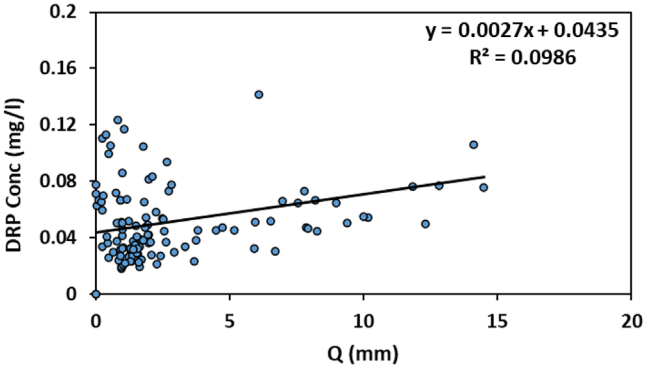

FIGURE 7 Flow-weighted daily mean dissolved reactive P concentrations (DRP conc) for the study site in water year 2019 plotted against tile discharge (Q)

Multiple linear regression analysis suggests that including both pathway and connectivity partitioning was important for estimating tile drainage DRP concentrations (Table 2; Figure 8). The p value of the F statistic for all three models was $<2 \times 10^{-16}$, suggesting all models were significant predictors of tile DRP concentrations. Further, all beta coefficients were found to be significant at a .05 significance level. Comparing the visual results of predicted DRP values and measured DRP values (Figure 8) illustrates that our new pathway-connectivity framework provided improvements at low-moderate DRP concentrations (<0.05) as evidenced by datapoints converging on the 1:1 line (Figure 8c). Further indication of improvement of prediction using our pathway-connectivity framework is evidenced by increases in the NSE (0.46; see Moriasi et al., 2007), as compared with SC-EMMA (0.41; Figure 8b), and hydrograph recession (0.27) results (Figure 8a). Although the improvement may partially reflect additional variables in the regression analysis, all regression variables were significant (Table 2), and the coefficients differed between each of the hydrograph partitions. This methodology may become particularly important for understanding dynamics at sites where matrix exchange of old water to macropores constitutes a greater proportion of the tile hydrograph. Further, this methodology may help with evaluating drivers of DRP delivery to tile at sites where new water is

TABLE 2 Results of the multiple linear regression analysis for daily flow weighted mean dissolved reactive P (DRP) concentrations

DRP	Estimated coefficients	*p* value of flow fractions	p value of overall model
Regression using new pathway-connectivity framework			
$DRP_{quick\text{-}old}$	.076 (.02)***	.00033	$<2 \times 10^{-16}$
$DRP_{quick\text{-}new}$	.091 (.008)****	$<2 \times 10^{-16}$	
$DRP_{slow\text{-}old}$	.028 (.003)****	2.65×10^{-12}	
$DRP_{slow\text{-}new}$	.153 (.019)****	8.8×10^{-13}	
Regression using only hydrograph recession analysis			
DRP_{quick}	.088 (.006)****	$<2 \times 10^{-16}$	$<2 \times 10^{-16}$
DRP_{slow}	.043 (.003)****	$<2 \times 10^{-16}$	
Regression using only specific conductance end-member mixing analysis			
DRP_{new}	.108 (.007)****	$<2 \times 10^{-16}$	$<2 \times 10^{-16}$
DRP_{old}	.034 (.003)****	$<2 \times 10^{-16}$	

Note. Estimated coefficient column shows estimated dissolved reactive P concentration (mg L^{-1}) associated with each flow fraction with standard error in parentheses
***Significant at the .001 probability level. ***Significant at the .0001 probability level.

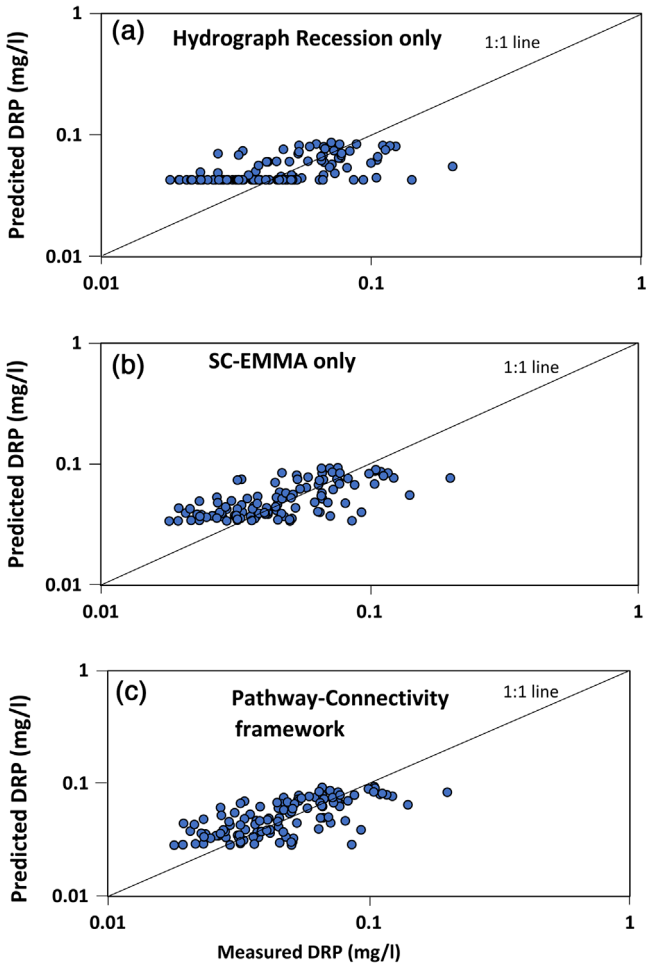

FIGURE 8 Multiple linear regression analysis results for daily flow-weighted mean concentrations of dissolved reactive P (DRP) as compared with (a) hydrograph recession results, (b) specific conductance end-member mixing analysis (SC-EMMA) results, and (c) the new pathway-connectivity framework results

a poor predictor of DRP concentrations (Pluer et al., 2020). Although predictions could be improved by accounting for variability in individual source compositions, our results support the importance of considering both hydrologic source and pathway to accurately predict DRP concentration dynamics. Furthermore, our analysis reflects an average DRP concentration from pathways; however, between events, there are likely complex sorption–desorption and solute diffusion dynamics that result in variability in each pathway. Considering redox or other conditions that can effect sorption–desorption dynamics between events can reduce uncertainty associated with our MLR analysis and improve the NSE value.

Best-fit concentrations from the regression model provide insight into sources of DRP in the soil profile and the impacts of preferential flow on groundwater recharge. Results of the regression analysis showed $DRP_{quick\text{-}old}$ was slightly less than $DRP_{quick\text{-}new}$. This result suggests $DRP_{quick\text{-}old}$ was initiated from near-surface matrix waters, given that water extractable P is highly stratified at the study site (see study site description). Such stratification and subsurface labile P accumulation is typical of tile-drained agroecosystems in the region (King et al., 2015; Xu et al., 2020). Additionally, concentrations for $DRP_{slow\text{-}new}$ were high, similar to quick-flow pathways. This finding was somewhat surprising considering that the slow-new source ultimately drains through the matrix reservoir. In part, this finding may partially reflect uncertainties in the new water SC end-member, particularly later in the event when SC values may be nonconservative (Vidon & Cuadra, 2010). Nevertheless, the finding is of interest because it suggests groundwater recharge through preferential flowpaths is an important source of greater DRP concentrations in tile drainage, which is rarely emphasized in tile DRP studies (King et al., 2015) and merits further consideration in future tile drainage water quality research, particularly when studying practices such as

drainage water management which directly affects water table dynamics.

The results of this study highlight that coupled characterization of flow pathway and water source are important for predicting DRP concentrations in tile drainage. Few studies have assessed the impact of flow pathway and source connectivity dynamics on tile P concentrations during storm events (Jiang et al., 2021). Previous studies have either used total Q, preferential flow, or new/old water estimates to predict P concentrations and loading in tiles. For instance, Pluer et al. (2020) found that preferential flow (estimated by conductivity based unmixing) was weakly correlated with P concentration, although the relationship between P and preferential flow was positive suggesting that preferential flow was a significant driver of P transport to tiles (Grant et al., 2019; Pluer et al., 2020). Given the relatively low cost of specific conductance, flow, and temperature sensors, widespread application of pathway-connectivity frameworks across environmental and management gradients has significant potential for advancing our understanding of contaminant transport in tile-drainage.

4 | CONCLUSIONS

A new method was presented that combines SC-EMMA and hydrograph recession approaches to describe both hydrologic pathways and source connectivity by separation of subsurface hydrograph into $Q_{\text{quick-new}}$, $Q_{\text{quick-old}}$, $Q_{\text{slow-new}}$, and $Q_{\text{slow-old}}$. Results highlight event-to-event and seasonal variability in dominant source-pathway dynamics. New water and quick flow hydrographs often differed in terms of peak timing and magnitude between events. Our results support that new water through macropore flow can occur under both dry and saturated conditions. Likewise, matrix–macropore exchange occurs under a range of antecedent conditions. Contributions of new water in the slow-flow reservoir highlighted that groundwater recharge plays a significant role in tile drainage fluxes.

Using the pathway-connectivity flow components as descriptors of DRP delivery in a MLR model improved prediction of DRP concentrations in tiles as compared with tile flow or hydrograph recession results, although it provided comparable results to new water and should be evaluated elsewhere at sites where matrix–macropore exchange constitute a larger percentage of the tile water budget. We found that new water that routes through quick-flow and slow-flow reservoirs play a significant role in delivery of DRP in tiles as compared to old water. Results show that DRP concentrations associated with matrix–macropore exchange revealed initiation of this water source from the near-surface matrix. This study highlights a data-driven approach using inexpensive sensors to assess flow pathway and connectivity dynamics and can be used to help inform numerical model evaluations and assess environmental gradients across sites in future work.

ACKNOWLEDGMENTS

The authors would like to thank three anonymous reviewers for their comments and suggestions, which greatly improved the quality of the manuscript. The authors thank the landowners of the study sites who provided access to the field and management data; Jedediah Stinner, Katie Rumora, Marie Pollock, Phil Levison, Sara Henderson, and Christian Bower for help in data collection and site maintenance; and Eric Fischer, Katie Emmett, and Whitney Phelps for laboratory analysis of water samples. Current funding for the USDA-ARS edge-of-field research network is in part through the NRCS Conservation Effects Assessment Project (CEAP).

AUTHOR CONTRIBUTIONS

Saeid Nazari: Conceptualization; Formal analysis; Investigation; Methodology; Writing-original draft. William I. Ford: Conceptualization; Data curation; Funding acquisition; Methodology; Supervision; Writing-original draft; Writing-review & editing. Kevin W. King: Data curation; Funding acquisition; Resources; Writing-review & editing.

CONFLICT OF INTEREST

The authors declare no conflict of interest.

ORCID

William I. Ford https://orcid.org/0000-0001-7940-9826

REFERENCES

Askar, M. H., Youssef, M. A., Chescheir, G. M., Negm, L. M., King, K. W., Hesterberg, D. L., & Skaggs, R. W. (2020). DRAINMOD Simulation of macropore flow at subsurface drained agricultural fields: Model modification and field testing. *Agricultural Water Management*., *242*, 106401. https://doi.org/10.1016/j.agwat.2020.106401

Beven, K., & Germann, P. (2013). Macropores and water flow in soils revisited. *Water Resources Research*, *49*(6), 3071–3092. https://doi.org/10.1002/wrcr.20156

Bishop, J. M., Callaghan, M. V., Cey, E. E., & Bentley, L. R. (2015). Measurement and simulation of subsurface tracer migration to tile drains in low permeability, macroporous soil. *Water Resources Research*, *51*(6), 3956–3981. https://doi.org/10.1002/2014WR016310

Brauer, C. C., Teuling, A. J., Torfs, P. J. J. F., & Uijlenhoet, R. (2014). The Wageningen Lowland Runoff Simulator (WALRUS): A lumped rainfall–runoff model for catchments with shallow groundwater. *Geoscientific Model Development*, *7*(5), 2313–2332. https://doi.org/10.5194/gmd-7-2313-2014

Callaghan, M. V., Head, F. A., Cey, E. E., & Bentley, L. R. (2017). Salt leaching in fine-grained, macroporous soil: Negative effects of excessive matrix saturation. *Agricultural Water Management*, *181*, 73–84. https://doi.org/10.1016/j.agwat.2016.11.025

Cey, E. E., & Rudolph, D. L. (2009). Field study of macropore flow processes using tension infiltration of a dye tracer in partially saturated

soils. *Hydrological Processes: An International Journal*, *23*(12), 1768–1779. https://doi.org/10.1002/hyp.7302

Cuthbert, M. O., Mackay, R., & Nimmo, J. R. (2013). Linking soil moisture balance and source-responsive models to estimate diffuse and preferential components of groundwater recharge. *Hydrology and Earth System Sciences*, *17*(3), 1003–1019. https://doi.org/10.5194/hess-17-1003-2013

Demand, D., Selker, J. S.,&, & Weiler, M. (2019). Influences of macropores on infiltration into seasonally frozen soil. *Vadose Zone Journal*, *18*, 180147. https://doi.org/10.2136/vzj2018.08.0147

Djabelkhir, K., Lauvernet, C., Kraft, P., & Carluer, N. (2017). Development of a dual permeability model within a hydrological catchment modeling framework: 1D application. *Science of the Total Environment*, *575*, 1429–1437. https://doi.org/10.1016/j.scitotenv.2016.10.012

Eckhardt, K. (2005). How to construct recursive digital filters for baseflow separation. *Hydrological Processes: An International Journal*, *19*(2), 507–515. https://doi.org/10.1002/hyp.5675

Flury, M., Flühler, H., Jury, W. A., & Leuenberger, J. (1994). Susceptibility of soils to preferential flow of water: A field study. *Water Resources Research*, *30*(7), 1945–1954. https://doi.org/10.1029/94WR00871

Ford, W., Williams, M. R., Young, M. B., King, K. W., & Fischer, E. (2018). Assessing intra-event phosphorus dynamics in drainage water using phosphate stable oxygen isotopes. *Transactions of the ASABE*, *61*(4), 1379–1392. https://doi.org/10.13031/trans.12804

Ford, W. I., Husic, A., Fogle, A., & Taraba, J. (2019). Long-term assessment of nutrient flow pathway dynamics and in-stream fate in a temperate karst agroecosystem watershed. *Hydrological Processes*, *33*(11), 1610–1628. https://doi.org/10.1002/hyp.13427

Ford, W. I., King, K. W., Williams, M. R., & Jr C., & R, B. (2017). Modified APEX model for simulating macropore phosphorus contributions to tile drains. *Journal of Environmental Quality*, *46*(6), 1413–1423. https://doi.org/10.2134/jeq2016.06.0218

Frey, S. K., Hwang, H. T., Park, Y. J., Hussain, S. I., Gottschall, N., Edwards, M., & Lapen, D. R. (2016). Dual permeability modeling of tile drain management influences on hydrologic and nutrient transport characteristics in macroporous soil. *Journal of Hydrology*, *535*, 392–406. https://doi.org/10.1016/j.jhydrol.2016.01.073

Frey, S. K., Rudolph, D. L., & Conant Jr, B. (2012). Bromide and chloride tracer movement in macroporous tile-drained agricultural soil during an annual climatic cycle. *Journal of Hydrology*, *460*, 77–89. https://doi.org/10.1016/j.jhydrol.2012.06.041

Gerke, H. H., Dusek, J., & Vogel, T. (2013). Solute mass transfer effects in two-dimensional dual-permeability modeling of bromide leaching from a tile-drained field. *Vadose Zone Journal*, *12*(2), vzj2012-0091. https://doi.org/10.2136/vzj2012.0091

Graham, C. B., & Lin, H. S. (2011). Controls and frequency of preferential flow occurrence: A 175-event analysis. *Vadose Zone Journal*, *10*(3), 816–831. https://doi.org/10.2136/vzj2010.0119

Granger, R. J., Gray, D. M., & Dyck, G. E. (1984). Snowmelt infiltration to frozen prairie soils. *Canadian Journal of Earth Sciences*, *21*, 669–677. https://doi.org/10.1139/e84-073

Grant, K. N., Macrae, M. L., & Ali, G. A. (2019). Differences in preferential flow with antecedent moisture conditions and soil texture: Implications for subsurface P transport. *Hydrological Processes*, *33*(15), 2068–2079. https://doi.org/10.1002/hyp.13454

Gregor, M., & Malik, P. (2012). *RC 4.0 user's manual, HydroOffice software package for water science*. HydroOffice. https://hydrooffice.org

Heathwaite, A. L., & Dils, R. M. (2000). Characterizing phosphorus loss in surface and subsurface hydrological pathways. *Science of the Total Environment*, *251*, 523–538. https://doi.org/10.1016/S0048-9697(00)00393-4

Heppell, C. M., & Chapman, A. S. (2006). Analysis of a two-component hydrograph separation model to predict herbicide runoff in drained soils. *Agricultural Water Management*, *79*(2), 177–207. https://doi.org/10.1016/j.agwat.2005.02.008

Husic, A., Fox, J., Adams, E., Ford, W., Agouridis, C., Currens, J., & Backus, J. (2019). Nitrate pathways, processes, and timing in an agricultural karst system: Development and application of a numerical model. *Water Resources Research*, *55*(3), 2079–2103. https://doi.org/10.1029/2018WR023703

Jiang, X., Livi, K. J., Arenberg, M. R., Chen, A., Chen, K. Y., Gentry, L., & Arai, Y. (2021). High flow event induced the subsurface transport of particulate phosphorus and its speciation in agricultural tile drainage system. *Chemosphere*, *263*, 128147. https://doi.org/10.1016/j.chemosphere.2020.128147

Kienzler, P. M., & Naef, F. (2008). Subsurface storm flow formation at different hillslopes and implications for the 'old water paradox.' *Hydrological Processes: An International Journal*, *22*(1), 104–116. https://doi.org/10.1002/hyp.6687

King, K. W., Fausey, N. R., & Williams, M. R. (2014). Effect of subsurface drainage on streamflow in an agricultural headwater watershed. *Journal of Hydrology*, *519*, 438–445. https://doi.org/10.1016/j.jhydrol.2014.07.035

King, K. W., Williams, M. R., Macrae, M. L., Fausey, N. R., Frankenberger, J., Smith, D. R., & Brown, L. C. (2015). Phosphorus transport in agricultural subsurface drainage: A review. *Journal of Environmental Quality*, *44*(2), 467–485. https://doi.org/10.2134/jeq2014.04.0163

Klaus, J., Zehe, E., Elsner, M., Külls, C., & McDonnell, J. J. (2013). Macropore flow of old water revisited: Experimental insights from a tile-drained hillslope. *Hydrology and Earth System Sciences*, *17*(1), 103–118. https://doi.org/10.5194/hess-17-103-2013

Kleinman, P. J., & Sharpley, A. N. (2002). Estimating soil phosphorus sorption saturation from Mehlich-3 data. *Communications in Soil Science and Plant Analysis*, *33*(11-12), 1825–1839. https://doi.org/10.1081/CSS-120004825

Kleinman, P. J., Sharpley, A. N., Withers, P. J., Bergström, L., Johnson, L. T., & Doody, D. G. (2015). Implementing agricultural phosphorus science and management to combat eutrophication. *AMBIO*, *44*(2), 297–310. https://doi.org/10.1007/s13280-015-0631-2

Kronholm, S. C., & Capel, P. D. (2015). A comparison of high-resolution specific conductance-based end-member mixing analysis and a graphical method for baseflow separation of four streams in hydrologically challenging agricultural watersheds. *Hydrological Processes*, *29*(11), 2521–2533. https://doi.org/10.1002/hyp.10378

Lee, L. J. E., Lawrence, D. S. L., & Price, M. (2006). Analysis of water-level response to rainfall and implications for recharge pathways in the Chalk aquifer, SE England. *Journal of Hydrology*, *330*(3–4), 604–620. https://doi.org/10.1016/j.jhydrol.2006.04.025

Lyne, V., & Hollick, M. (1979). Stochastic time-variable rainfall-runoff modelling. In *Proceedings of the Hydrology and Water Resources Symposium* (pp. 89–92). Institution of Engineers Australia.

Malík, P., & Vojtková, S. (2012). Use of recession-curve analysis for estimation of karstification degree and its application in assessing overflow/underflow conditions in closely spaced karstic springs. *Environmental Earth Sciences*, *65*(8), 2245–2257. https://doi.org/10.1007/s12665-012-1596-0

Mellander, P. E., Jordan, P., Melland, A. R., Murphy, P. N., Wall, D. P., Mechan, S.,&, & Shortle, G. (2013). Quantification of phosphorus transport from a karstic agricultural watershed to emerging spring water. *Environmental Science & Technology*, *47*(12), 6111–6119. https://doi.org/10.1021/es304909y

Mirus, B. B., & Nimmo, J. R. (2013). Balancing practicality and hydrologic realism: A parsimonious approach for simulating rapid groundwater recharge via unsaturated-zone preferential flow. *Water Resources Research*, *49*(3), 1458–1465. https://doi.org/10.1002/wrcr.20141

Mohammed, A. A., Cey, E. E., Hayashi, M., Callaghan, M. V., Park, Y. J., Miller, K. L., & Frey, S. K. (2021). Dual-permeability modeling of preferential flow and snowmelt partitioning in frozen soils. *Vadose Zone Journal*, *20*(2), e20101. https://doi.org/10.1002/vzj2.20101

Mohammed, A. A., Kurylyk, B. L., Cey, E. E., & Hayashi, M. (2018). Snowmelt infiltration and macropore flow in frozen soils: Overview, knowledge gaps, and a conceptual framework. *Vadose Zone Journal*, *17*, 180084. https://doi.org/10.2136/vzj2018.04.0084

Moriasi, D. N., Arnold, J. G., Van Liew, M. W., Bingner, R. L., Harmel, R. D., & Veith, T. L. (2007). Model evaluation guidelines for systematic quantification of accuracy in watershed simulations. *Transactions of the ASABE*, *50*(3), 885–900. https://doi.org/10.13031/2013.23153

Murphy, J., & Riley, J. P. (1962). A modified single solution method for the determination of phosphate in natural waters. *Analytica Chimica Acta*, *27*, 31–36.

Nazari, S., Ford, W. I., & King, K. W. (2020). Impacts of preferential flow and agroecosystem management on subsurface particulate phosphorus loadings in tile-drained landscapes. *Journal of Environmental Quality*, *49*(5), 1370–1383. https://doi.org/10.1002/jeq2.20116

Nimmo, J. R. (2012). Preferential flow occurs in unsaturated conditions. *Hydrological Processes*, *26*(5), 786–789. https://doi.org/10.1002/hyp.8380

Ortega-Pieck, A., Norby, J., Brooks, E. S., Strawn, D., Crump, A. R., & Huggins, D. R. (2020). Sources and subsurface transport of dissolved reactive phosphorus in a semiarid, no-till catchment with complex topography. *Journal of Environmental Quality*, *49*(5), 1286–1297. https://doi.org/10.1002/jeq2.20114

Pferdmenges, J., Breuer, L., Julich, S., & Kraft, P. (2020). Review of soil phosphorus routines in ecosystem models. *Environmental Modelling & Software*, *126*, 104639. https://doi.org/10.1016/j.envsoft.2020.104639

Pilgrim, D. H., & Huff, D. D. (1983). Suspended sediment in rapid subsurface stormflow on a large field plot. *Earth Surface Processes and Landforms*, *8*(5), 451–463. https://doi.org/10.1002/esp.3290080506

Pittman, F., Mohammed, A., & Cey, E. (2020). Effects of antecedent moisture and macroporosity on infiltration and water flow in frozen soil. *Hydrological Processes*, *34*, 795–809. https://doi.org/10.1002/hyp.13629

Pluer, W. T., Macrae, M., Buckley, A., & Reid, K. (2020). Contribution of preferential flow to tile drainage varies spatially and temporally. *Vadose Zone Journal*, *19*, e20043. https://doi.org/10.1002/vzj2.20043

Rimmer, A., & Hartmann, A. (2012). Simplified conceptual structures and analytical solutions for groundwater discharge using reservoir equations. *Water Resources Management and Modeling*, *2*, 217–238.

Schilling, K. E., & Helmers, M. (2008). Tile drainage as karst: Conduit flow and diffuse flow in a tile-drained watershed. *Journal of Hydrology*, *349*(3–4), 291–301. https://doi.org/10.1016/j.jhydrol.2007.11.014

Schilling, K. E., Streeter, M. T., Vogelgesang, J., Jones, C. S., & Seeman, A. (2020). Subsurface nutrient export from a cropped field to an agricultural stream: Implications for targeting edge-of-field practices. *Agricultural Water Management*, *241*, 106339. https://doi.org/10.1016/j.agwat.2020.106339

Simard, R. R., Beauchemin, S., & Haygarth, P. M. (2000). Potential for preferential pathways of phosphorus transport. *Journal of Environmental Quality*, *29*(1), 97–105. https://doi.org/10.2134/jeq2000.00472425002900010012x

Sklash, M. G., & Farvolden, R. N. (1979). The role of groundwater in storm runoff. *Journal of Hydrology*, *43*(1-4), 45–65. https://doi.org/10.1016/0022-1694(79)90164-1

Smith, E. A., & Capel, P. D. (2018). Specific conductance as a tracer of preferential flow in a subsurface-drained field. *Vadose Zone Journal*, *17*, 170206. https://doi.org/10.2136/vzj2017.11.0206

Snyder, L., Potter, J. D., & McDowell, W. H. (2018). An evaluation of nitrate, fDOM, and turbidity sensors in New Hampshire streams. *Water Resources Research*, *54*(3), 2466–2479. https://doi.org/10.1002/2017WR020678

Soil Survey Staff. (2019). *Web soil survey*. USDA-NRCS. https://websoilsurvey.nrcs.usda.gov/

Stadler, D., Flühler, H., & Jansson, P. E. (1997). Modelling vertical and lateral water flow in frozen and sloped forest soil plots. *Cold Regions Science and Technology*, *26*, 181–194. https://doi.org/10.1016/S0165-232X(97)00017-7

Stadler, D., Stähli, M., Aeby, P., & Flühler, H. (2000). Dye tracing and image analysis for quantifying water infiltration into frozen soils. *Soil Science Society of America Journal*, *64*(2), 505–516. https://doi.org/10.2136/sssaj2000.642505x

Stamm, C. H., Flühler, H., Gächter, R., Leuenberger, J., & Wunderli, H. (1998). Preferential transport of phosphorus in drained grassland soils. *Journal of Environmental*, *27*(3), 515–522. https://doi.org/10.2134/jeq1998.00472425002700030006x

Tokunaga, T. K., & Wan, J. (1997). Water film flow along fracture surfaces of porous rock. *Water Resources Research*, *33*(6), 1287–1295. https://doi.org/10.1029/97WR00473

Van Esbroeck, C. J., Macrae, M. L., Brunke, R. I., & McKague, K. (2016). Annual and seasonal phosphorus export in surface runoff and tile drainage from agricultural fields with cold temperate climates. *Journal of Great Lakes Research*, *42*(6), 1271–1280. https://doi.org/10.1016/j.jglr.2015.12.014

Vidon, P., & Cuadra, P. E. (2010). Impact of precipitation characteristics on soil hydrology in tile-drained landscapes. *Hydrological Processes*, *24*(13), 1821–1833. https://doi.org/10.1002/hyp.7627

Watanabe, K., & Kugisaki, Y. (2017). Effect of macropores on soil freezing and thawing with infiltration. *Hydrological Processes*, *31*, 270–278. https://doi.org/10.1002/hyp.10939

Williams, M. R., King, K. W., & Fausey, N. R. (2015). Drainage water management effects on tile discharge and water quality. *Agricultural Water Management*, *148*, 43–51. https://doi.org/10.1016/j.agwat.2014.09.017

Williams, M. R., King, K. W., Ford, W., Buda, A. R., & Kennedy, C. D. (2016). Effect of tillage on macropore flow and phosphorus transport to tile drains. *Water Resources Research*, *52*(4), 2868–2882. https://doi.org/10.1002/2015WR017650

Wright, R. B., Lockaby, B. G., & Walbridge, M. R. (2001). Phosphorus availability in an artificially flooded southeastern floodplain forest soil. *Soil Science Society of America Journal*, *65*(4), 1293–1302. https://doi.org/10.2136/sssaj2001.6541293x

Xu, S., Gentry, L., Chen, K. Y., & Arai, Y. (2020). Intensive agricultural management-induced subsurface accumulation of labile phosphorus in midwestern agricultural soils dominated by tile lines. *Soil Science Society of America Journal*, *84*(4), 1094–1109. https://doi.org/10.1002/saj2.20089

Xylem/YSI incorporation. (2020). *EXO user manual*. Xylem/YSI incorporation. https://www.ysi.com/file%20library/documents/manuals/exo-user-manual-web.pdf

How to cite this article: Nazari, S, Ford, WI, & King, KW. Quantifying hydrologic pathway and source connectivity dynamics in tile drainage: Implications for phosphorus concentrations. *Vadose Zone J.* 2021;*20:*e20154. https://doi.org/10.1002/vzj2.20154